Fenofibrate attenuates the cytotoxic effect of cisplatin on lung cancer cells by enhancing the antioxidant defense system *in vitro*

MARIKO KOGAMI[1,2], SHINJI ABE[2], HIROYUKI NAKAMURA[1] and KAZUTETSU AOSHIBA[1]

[1]Department of Respiratory Medicine, Tokyo Medical University Ibaraki Medical Center, Ami, Ibaraki 300-0395;
[2]Department of Respiratory Medicine, Tokyo Medical University, Tokyo 160-0023, Japan

Abstract. Fenofibrate (FF) is a peroxisome proliferator-activated receptor (PPAR)-α agonist that is widely used for the treatment of hyperlipidemia. It has been shown to have pleiotropic actions beyond its hypolipidemic effect. FF has been shown to exert a cytotoxic effect on some cancer cells when used at higher than clinically relevant concentrations; on the other hand, its cytoprotective effect on normal cells has also been reported. The present study assessed the effect of FF on cisplatin (CDDP) cytotoxicity to lung cancer cells *in vitro*. The results demonstrated that the effect of FF on lung cancer cells depends on its concentration. FF at ≤ 50 μM, which is a clinically achievable blood concentration, attenuated CDDP cytotoxicity to lung cancer cells, whereas FF at ≥ 100 μM, albeit clinically unachievable, had an anticancer effect. The mechanism of FF attenuation of CDDP cytotoxicity involved PPAR-α-dependent aryl hydrocarbon receptor (AhR) expression, which in turn stimulated nuclear factor erythroid 2-related factor 2 (Nrf2) expression and antioxidant production, resulting in lung cancer cell protection from CDDP-evoked oxidative damage. In conclusion, the present study revealed that FF, at clinically relevant concentrations, attenuated CDDP cytotoxicity to lung cancer cells by enhancing the antioxidant defense system through activation of a pathway that involves the PPAR-α-PPAR response element-AhR xenobiotic response element-Nrf2-antioxidant response element. These findings suggested that concomitant use of FF with CDDP may compromise the efficacy of chemotherapy. Although the anticancer property of FF has recently attracted much attention, concentrations that exceed clinically relevant concentrations are required.

Correspondence to: Professor Kazutetsu Aoshiba, Department of Respiratory Medicine, Tokyo Medical University Ibaraki Medical Center, 3-20-1 Chuou, Ami-machi, Inashiki-gun, Ibaraki 300-0395, Japan
E-mail: kaoshiba@tokyo-med.ac.jp

Abbreviations: AhR, aryl hydrocarbon receptor; ANOVA, analysis of variance; ARE, antioxidant response element; ARNT, AhR nuclear translocator; BSA, bovine serum albumin; FBS, fetal bovine serum; PBS, phosphate buffered saline; PPAR, peroxisome proliferator-activated receptor; PPRE, PPAR response element; ROS, reactive oxygen species; XRE, xenobiotic response element

Introduction

Fenofibrate (FF), which is a peroxisome proliferator-activated receptor (PPAR)-α agonist (1), has been widely used for the treatment of hyperlipidemia since 1975 (2,3). *In vivo*, FF is rapidly converted to fenofibric acid, which binds to PPAR-α and forms a heterodimer complex with retinoid X receptor. This complex then binds to PPAR response element (PPRE) to activate transcription of target genes, including that of lipid metabolism regulation (4). Beyond its hypolipidemic effect, FF has been shown to have pleiotropic actions in a PPAR-α-dependent or independent manner. Among them, the anticancer property of FF has attracted much attention as a new option for therapy (5). According to previous reports, FF had cytotoxic effects on various tumor cell lines derived from the brain, breast, liver, prostate, and lungs by inducing apoptosis, cell cycle arrest, and motility inhibition (5). However, in some of the studies, FF concentrations that were higher than clinically relevant blood concentrations (i.e., ≤ 50 μM) were used to exert anticancer effects; interpretation of this result requires some caution (6,7). Furthermore, no studies have evaluated the anticancer effect of FF in combination with standard chemotherapeutic drugs, such as cisplatin (CDDP) (8).

On the other hand, other in *in vitro* and *in vivo* experiments, including animal models of diabetic retinopathy and nephropathy and ischemia/ reperfusion-induced cardiac injury, demonstrated that FF has a cytoprotective effect on normal cells (4,9). Although the mechanism of FF-induced cytoprotection is uncertain, it was reported to involve enhancement of antioxidants. For example, FF has been shown to attenuate oxidative damage to cardiomyocytes, retinal endothelial cells, auditory hair cells, and skin keratinocytes (10-13). Moreover, FF has been reported to reduce CDDP toxicity to renal tubular cells and auditory hair cells, both of which can be adversely affected by CDDP-containing chemotherapy (14,15). Because oxidative stress comprises the major mechanism of CDDP chemotherapy (16), we hypothesized that concurrent treatment with FF may attenuate the anticancer effect of CDDP.

Because both hyperlipidemia and cancer have become increasingly prevalent, not a few patients with hyperlipidemia and receiving FF need to commence chemotherapy for cancer. Therefore, elucidating the impact of FF on CDDP chemotherapy is clinically important. In this study, we determined the effect of FF at clinically relevant blood concentrations on CDDP cytotoxicity to lung cancer cells *in vitro*.

Materials and methods

Cell culture. Human non-small lung cancer cell lines A549 (CCL-185), H1299 (CRL-5803) and H441 (HTB-174) were obtained from the American Type Culture Collection (Manassas, VA, USA); PC3 (JCRB0077) was obtained from the Japanese Collection of Research Bioresources Cell Bank (Osaka, Japan). The cell lines were authenticated by short tandem repeat profiling using the Promega PowerPlex® 16 HS system (Promega Corporation, Madison, WI). A549 cells were grown and maintained on type I collagen-coated plates in Dulbecco's Modified Eagle medium (Gibco; Thermo Fisher Scientific, Inc., Waltham, MA, USA) containing 10% fetal bovine serum (FBS, Biowest, Nuaillé, France). H1299 and PC3 cells were grown and maintained in Roswell Park Memorial Institute (RPMI) 1640 medium (Gibco; Thermo Fisher Scientific, Inc.) containing 10% FBS. The cells were incubated at 37°C in a humidified incubator saturated with a gas mixture containing 5% CO_2. Confluent cells were treated with the following: i) FF (0-200 μM or 50 μM unless otherwise indicated; Sigma-Aldrich Japan, Tokyo, Japan); ii) WY14643 (WY, 0-50 μM or 50 μM unless otherwise indicated; Cayman Chemical, Ann Arbor, MI, USA); or iii) vehicle alone (0.2% dimethyl sulfoxide) in RPMI1640 containing 0.5% FBS. CDDP (0-40 μM or 40 μM unless otherwise indicated; Nippon Kayaku Co., Ltd., Tokyo, Japan) was added to the culture medium after 12-48 h of treatment with FF or WY.

Cell survival assay. Cell survival was evaluated by Hoechst 33342 DNA quantification assay, a colorimetric alamarBlue® assay, and ATP quantification assay. For the Hoechst 33342 DNA quantification assay, cells that were cultured in a 96-well plate were lysed in 100 μl of distilled water, followed by a freeze-thaw cycle. Thereafter, the cell lysates were solubilized in 100 μl of TNE buffer (i.e., 10 mM Tris, 1 mM EDTA, and 2 M NaCl; pH 7.4) containing 10 μg/ml of Hoechst 33342 (Sigma-Aldrich Japan, Tokyo, Japan). The fluorescence intensities were read at an excitation (Ex) of 350 nm and emission (Em) of 460 nm using a microplate fluorometer (PerkinElmer Arvo X2, PerkinElmer Japan Co., Ltd., Tokyo, Japan). For the alamarBlue® assay, a one-tenth volume of alamarBlue® reagent (Thermo Fisher Scientific) was added to the culture medium in a 96-well plate for the last four h of incubation. Thereafter, the absorbance was measured at 570 nm on a Benchmark Plus microplate immunoreader (Bio-Rad Laboratories, Inc., Hercules, CA, USA) using 600 nm as a reference wavelength. For the ATP quantification assay, the Cellno ATP assay reagent (Toyo B-Net, Co, Ltd., Tokyo, Japan) was used according to the manufacturer's instructions. Briefly, 100 μl of the lysis assay solution provided by the manufacturer was added to confluent cell cultures in a 96-well culture plate. After the plate was shaken for 1 min and incubated for 10 min at 23°C, luminescence was measured in microplate luminometer (PerkinElmer Arvo X2, PerkinElmer Japan Co., Ltd., Tokyo, Japan).

Measurement of cellular reactive oxygen species (ROS) levels. A549 cells in 96-well plates were treated with or without FF (50-μM) or WY (50-μM) for 12 h, followed by exposure to 40-μM CDDP for 48 h in the presence or absence of FF and WY. The cells were then loaded with the cellular reactive oxygen species (ROS) sensor CellROX® Green (5-μM) (Thermo Fisher Scientific) for 30 min at 37°C in the presence of the nuclear dye Hoechst33342. The medium was replaced with phosphate buffered saline (PBS); the fluorescence intensities of the CellROX® Green (Ex 485 nm, Em 530 nm) and Hoechst33342 (Ex 355 nm, Em 460 nm) dyes were recorded using microplate fluorometer. The fluorescence intensities of CellROX® Green were normalized to Hoechst33342 fluorescence in the corresponding wells.

Superoxide dismutase assay. Cellular superoxide dismutase (SOD) activity was determined using an SOD assay kit-WST (Dojindo Laboratories, Kumamoto, Japan), according to the manufacturer's instructions.

Catalase activity assay. Cellular catalase activity was determined using the EnzyChrom catalase assay kit (BioAssay Systems, Hayward, CA, USA), according to the manufacturer's instructions.

Western blotting. Cell samples were lysed in a radioimmunoprecipitation assay (RIPA) buffer [50 mM Tris hydrochloride, 150 mM NaCl, 0.4 mM EDTA, 0.5% Nonidet P-40, and 0.1% sodium dodecyl sulfate (SDS); pH 7.4] containing a protease inhibitor cocktail (Sigma-Aldrich Japan), a phosphatase inhibitor cocktail (Santa Cruz Biotechnology, Santa Cruz, CA, USA) and sodium orthovanadate (1 mM). Nuclear proteins and cytoplasmic proteins were extracted using a nuclear extraction kit (Active Motif, Carlsbad, CA, USA), according to the manufacturer's instructions. The samples were centrifuged at 10,000 x g for 30 min, and the total protein concentration in the supernatants was assessed using the DC protein assay kit (Bio-Rad Laboratories). After combining with 5X SDS sample buffer (500 mM Tris, 5% 2-mercaptoethanol, 10% glycerin, 2.5% SDS, 0.0125% bromophenol blue; pH 6.8), the samples (20-μg protein/lane) were fractionated by SDS-polyacrylamide gel electrophoresis and transferred to a polyvinylidene difluoride membrane (EMD Millipore Immobilon®-P; Millipore, Co., Billerica, MA, USA). The membranes were blocked with 4% bovine serum albumin (BSA, Biowest); probed with the primary antibodies described below; diluted in an immunoreaction enhancer solution (Can Get Signal® Solution 1; Toyobo Co., Ltd., Osaka, Japan); and reacted with horseradish peroxidase (HRP)-conjugated secondary antibodies, such as stabilized goat anti-rabbit IgG (32460, Thermo Fisher Scientific) and stabilized goat anti-mouse IgG (32430, Thermo Fisher Scientific). The immune complexes were visualized using an enhanced chemiluminescence reagent (SuperSignal West Pico; Thermo Fisher Scientific). The signal intensities were quantified by densitometric scanning using ImageJ (version 1.49V; National Institutes of Health, Bethesda, MD, USA).

The primary antibodies used in this study were mouse monoclonal anti-β-actin (017-24573, Wako, Tokyo, Japan); rabbit polyclonal anti-Lamin B1 (12987-1-AP, Proteintech Group, Inc., Tokyo, Japan); rabbit polyclonal anti-α-tubulin (PM054-7, Medical & Biological Laboratories Co., Ltd., Tokyo, Japan); mouse monoclonal anti-p53 (sc-126, Santa Cruz Biotechnology), rabbit polyclonal anti-phosphorylated p53 (CSB-PA157242, Cusabio Biotech Co., Ltd., Houston, TX, USA); mouse monoclonal anti-heat shock protein 70 (HSP70) (SPA-810, Stressgen Biotechnologies Co., Ltd., Seoul, Korea); rabbit polyclonal anti-B-cell/CLL lymphoma 2 (Bcl-2) (12789-1-AP, Proteintech Group); rabbit polyclonal anti-B-cell lymphoma-extra large (Bcl-xL) (10783-1-AP, Proteintech Group); rabbit polyclonal anti-Bcl-2-associated X protein (Bax) (50599-2-Ig, Proteintech Group); mouse monoclonal anti-Bcl-2 antagonist of cell death (Bad) (B36420, BD Transduction Laboratories, Lexington, KY, USA); rabbit polyclonal anti-superoxide dismutase (SOD) 1 (GTX100554, GeneTex, Inc., Irvine, CA, USA); rabbit polyclonal anti-SOD2 (GTX116093, GeneTex); rabbit polyclonal anti-heme oxygenase (HO)-1 (GTX101147, GeneTex); rabbit polyclonal anti-catalase (GTX110704, GeneTex); rabbit monoclonal anti-nuclear factor erythroid 2-related factor 2 (Nrf2) (ab62352, Abcam, Cambridge, UK); mouse monoclonal anti-Kelch-like ECH-associated protein 1 (Keap1) (M224-3, Medical & Biological Laboratories Co., Ltd.); rabbit polyclonal anti-β-transduction repeat containing protein (β-TrCP) (GTX102667, GeneTex); rabbit polyclonal anti-aryl hydrocarbon receptor (AhR) (28727-1-AP, Proteintech Group); and mouse monoclonal anti-ubiquitin (sc-8017, Santa Cruz Biotechnology, Dallas, TX, USA).

Immunoprecipitation. Cells were lysed in Nonidet P-40 lysis buffer (50 mM Tris hydrochloride, 140 mM NaCl, 1% NP-40, and 10% glycerol; pH 7.5) containing a protease inhibitor cocktail (Sigma-Aldrich, Japan). Cell lysates containing an equal amount (820 μg) of protein were incubated with 1 μg of rabbit monoclonal anti-Nrf2 (ab62352, Abcam) and protein A/G plus agarose (sc-2003, Santa Cruz Biotechnology) on a rotator shaker at 4°C overnight. The beads were washed with RIPA buffer and boiled in 1X SDS sample buffer at 95°C for 5 min. Proteins were separated by sodium dodecyl sulfate-polyacrylamide gel electrophoresis and immunoblotted as described above.

Immunofluorescence staining. Cells in eight-chamber slides (Nunc® Lab-Tek II® Chamber Slide System; Thermo Fisher Scientific) were fixed with 3% paraformaldehyde and permeabilized with 0.5% Triton® X-100 (Nacalai tesque, Inc., Kyoto, Japan) in PBS for 10 min. After blocking the nonspecific binding sites with 3% BSA, the slides were incubated with mouse monoclonal anti-γH2A histone family member X (γH2AX) antibody (ab22551, Abcam), followed by alpaca anti-mouse IgG1 (VHH) conjugated with Alexa Fluor 488 (SA510328, Thermo Fisher Scientific) or rabbit polyclonal anti-AhR (28727-1-AP) then by alpaca antirabbit IgG (VHH) conjugated with Alexa Fluor 488 (SA510322, Thermo Fisher Scientific). Thereafter, the cell nuclei were counterstained with 4',6-diamidino-2-phenylindole (DAPI). Fluorescence images were obtained using a microscope (Olympus IX71; Olympus Optical Co., Ltd., Tokyo, Japan) equipped with a digital camera. For γH2AX DNA damage assay, the cells with ≥10 foci were determined to be positive. For foci quantification, 100 cells were counted in each sample, and percentages of the positive cells among the counted cells were calculated.

Transcription factor activation assay. Activation of the transcription factor Nrf2 was assessed using a TranAM® Nrf2 Transcription Factor Binding Assay kit (Active Motif Japan, Tokyo, Japan), according to the manufacturer's instructions.

Cycloheximide chase assay. A549 cells were treated with 50-μM FF for 36 h, followed by addition of 100 μg/ml of cycloheximide. After 0, 15, 30, and 60 min, the cells were lysed and processed for Western blot analysis using rabbit monoclonal anti-Nrf2 antibody (ab62352) and an HRP-conjugated secondary antibody. Signal intensities were quantified by densitometric scanning using ImageJ (version 1.49V). The half-lives ($T_{1/2}$) of Nrf2 were calculated from regression curve obtained from the plotted data of quantified signal intensities normalized to β-actin at each time point.

Measurement of cytochrome P450 1A1 activity. Cytochrome P450 1A1 (CYP1A1) activity was determined using P450-Glo CYP1A1 assay kit (Promega Corporation, Madison, WI, USA), according to the manufacturer's instructions. The P450-Glo assay value was normalized using CellTiter-Glo® Luminescent Cell Viability Assay (Promega Corporation).

Reverse transcription-quantitative polymerase chain reaction. This test was performed using TaqMan® Fast Advanced Cells-to-CT Kit (Thermo Fisher Scientific) and TaqMan® Gene Expression Assay (Thermo Fisher Scientific). The predesigned human-specific primers with TaqMan probes that were used in this study were ACTB TaqMan® Gene Expression Assay (FAM) (assay ID: Hs99999903_m1, Thermo Fisher Scientific); NFE2L2 TaqMan® Gene Expression Assay (FAM) (assay ID: Hs00975961_g1, Thermo Fisher Scientific); AHR TaqMan® Gene Expression Assay (FAM) (assay ID: Hs00169233_m1, Thermo Fisher Scientific); and PPARA TaqMan® Gene Expression Assay (FAM) (assay ID: Hs00947536_m1, Thermo Fisher Scientific) (Table I). The ΔΔCq method was used to calculate the fold gene expression of NFE2L2 or AhR. ACTB was used as a housekeeping gene to normalize the Ct values (17). The formulas used in this study were as follows: ΔCq=Cq (gene of interest)-Cq (housekeeping gene); ΔΔCq=ΔCq (Sample)-ΔCq (Control average); Fold gene expression=$2^{-(\Delta\Delta Cq)}$.

Small interfering RNA transfection. Knockdown of AhR and PPARA was achieved by treating A549 cells with small interfering RNA (siRNA) duplexes that comprised four different predesigned sequences that target the human AhR mRNA sequence (accession number P35869; cat. no. L-004990-00-0005; Horizon Discovery Ltd., Cambridge, UK) and the human PPARA mRNA sequence (accession number AY206718; cat. no. L-003434-00-0005; Horizon Discovery Ltd.) (Table II). For the control experiment, cells were treated with scrambled nontargeting siRNAs (catalogue no. D-001810-10; Horizon Discovery). siRNAs were transfected using a transfection reagent (DharmaFECT 1, Horizon Discovery), according to the manufacturer's instructions.

Table I. Reverse transcription-quantitative polymerase chain reaction-based TaqMan® gene expression assays.

Target	Exon boundaries	TaqMan gene expression assay ID	Accession no.
ACTB	1-1	Hs99999903_m1	NM_001101
NFE2L2	4-5	Hs00975961_g1	NM_006164
AHR	6-7	Hs00169233_m1	NM_001621
PPARA	4-5	Hs00947536_m1	NM_001001928

ACTB, actin β; NFE2L2, NFE2 like bZIP transcription factor 2 (nuclear factor erythroid 2-related factor 2); AHR, aryl hydrocarbon receptor; PPARA, peroxisome proliferator-activated receptor-α.

Table II. Sequences of the small interfering RNAs.

Target	Sequence
AHR	
Sense-1	5'-GCAAGUUAAUGGCAUGUUUUU-3'
Antisense-1	3'-UUCGUUCAAUUACCGUACAAA-5'
Sense-2	5'-GAACUCAAGCUGUAUGGUAUU-3'
Antisense-2	3'-UUCUUGAGUUCGACAUACCAU-5'
Sense-3	5'-GCACGAGAGGCUCAGGUUAUU-3'
Antisense-3	3'-UUCGUGCUCUCCGAGUCCAAU-5'
Sense-4	5'-GCAACAAGAUGAGUCUAUUUU-3'
Antisense-4	3'-UUCGUUGUUCUACUCAGAUAA-5'
PPARA	
Sense-1	5'-CCCGUUAUCUGAAGAGUUCUU-3'
Antisense-1	3'-UUGGGCAAUAGACUUCUCAAG-5'
Sense-2	5'-GCUUUGGCUUUACGGAAUAUU-3'
Antisense-2	3'-UUCGAAACCGAAAUGCCUUAU-5'
Sense-3	5'-GACUCAAGCUGGUGUAUGAUU-3'
Antisense-3	3'-UUCUGAGUUCGACCACAUACU-5'
Sense-4	5'-GGGAAACAUCCAAGAGAUUUU-3'
Antisense-4	3'-UUCCCUUUGUAGGUUCUCUAA-5'
Nontargeting	
Sense-1	5'-UGGUUUACAUGUCGACUAAUU-3'
Antisense-1	3'-UUACCAAAUGUACAGCUGAUU-5'
Sense-2	5'-UGGUUUACAUGUUGUGUGAUU-3'
Antisense-2	3'-UUACCAAAUGUACAACACACU-5'
Sense-3	5'-UGGUUUACAUGUUUUCUGAUU-3'
Antisense-3	3'-UUACCAAAUGUACAAAAGACU-5'
Sense-4	5'-UGGUUUACAUGUUUUCCUAUU-3'
Antisense-4	3'-UUACCAAAUGUACAAAAGGAU-5'

Each strand of the RNAs contains a 19-nucleotide target sequence, with a two-nucleotide UU overhang at the 3' end. A mixture of four siRNAs was used for each target gene. AHR, aryl hydrocarbon receptor; PPARA, peroxisome proliferator-activated receptor-α.

Statistical analysis. The mean and standard error of the mean were used to express the data. Statistical analyses were carried out using Microsoft Excel X with the Statcel 3 (OMS, Tokyo, Japan) add-in software. The Welch t-test, or one-way or two-way analysis of variance (ANOVA) was used as appropriate to determine significant differences. If the results of the ANOVA were significant, the Tukey-Kramer test or Dunnett's test was used as a post hoc for multiple comparisons. $P<0.05$ was considered to indicate a statistically significant difference.

Results

Dose-dependent effect of FF on lung cancer cell survival in the presence or absence of CDDP. We first examined whether treatment with FF at concentrations of 0-200 μM affected the survival of A549 cells. As shown in Fig. 1A, the Hoechst 33342 DNA assay and alamarBlue® assay showed that FF at ≥100 μM significantly reduced A549 cell survival. This result corroborated that of a previous research, which showed the anticancer effect of FF (5). However, at concentrations of ≤50 μM, which correspond to clinically achievable blood concentrations (7,18), FF had no significant effect on A549 cell survival. We next examined whether FF at ≤50 μM affected A549 cell survival in the presence of CDDP. Fig. 1B shows that exposure to 5-40 μM of CDDP reduced A549 cell survival. However, the presence of FF at 50 μM significantly promoted A549 cell survival after CDDP exposure, as shown by the Hoechst 33342 DNA, alamarBlue®, and cellular ATP assays. Within a FF concentration range of 25-50 μM, FF had a dose-dependent pro-survival effect against CDDP (Fig. 1C). In addition, treatment with WY, which is a selective agonist of PPAR-α, promoted A549 cell survival after CDDP exposure in a dose-dependent manner (Fig. 1C). The pro-survival effect of FF against CDDP was attenuated in the presence of the PPAR-α antagonist GW6471 (Fig. 1D), indicating that the pro-survival effect of FF against CDDP was, at least in part, secondary to its PPAR-α agonistic activity. These findings implied that FF at 25 or 50 μM had a cytoprotective effect on A549 cells against CDDP, whereas FF at ≥50 μM, albeit unachievable in clinical practice, had a cytotoxic effect. We also examined the effect of FF on other non-small cell lung cancer cell lines, including H1299, PC3, and H441, to determine whether the FF attenuation of CDDP cytotoxicity was peculiar to A549 cells. In each of these cell lines, treatment with FF at 50 μM reduced the CDDP-induced cell death (Fig. 1E).

FF treatment did not modulate the DNA damage response elicited by CDDP exposure. Next, we examined whether FF modulated CDDP-induced DNA damage, which is thought to contribute to the mechanism of CDDP cytotoxicity (16). CDDP exposure evoked a DNA damage response in A549 cells, as demonstrated by phosphorylation of H2AX
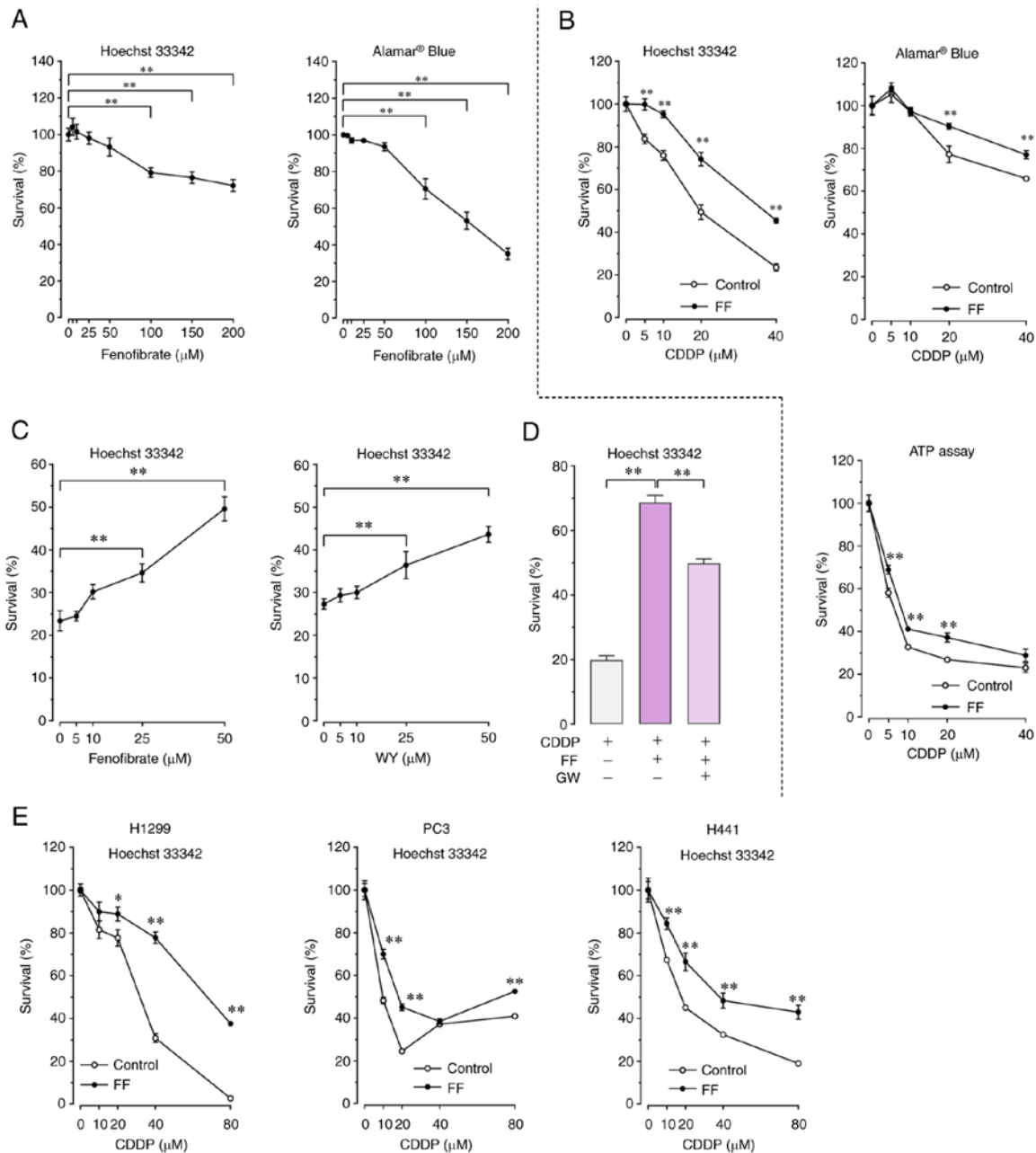
Figure 1. Dose-dependent effect of FF on A549 cell survival in the presence or absence of CDDP. (A) To study the effect of FF on cell survival in the absence of CDDP, A549 cells were treated with 5-200 μM of FF or vehicle alone for 72 h. Cell survival was determined by Hoechst 33342 DNA quantification assay (n=8) and alamarBlue® assay (n=8). Data are expressed as the mean and standard error of the mean. **P<0.01 using the one-way ANOVA and Dunnett's test. (B) To study the effect of FF on cell survival in the presence of CDDP, A549 cells were pretreated with 50-μM FF or vehicle alone for 12 h, followed by exposure to 40-μM CDDP for 72 h in the presence or absence of FF. Cell survival was determined by Hoechst 33342 DNA quantification assay (n=6), alamarBlue® assay (n=8), and ATP quantification assay (n=6). Data are expressed as the mean and standard error of the mean. **P<0.01 vs. control using the Welch t-test. (C) To study the dose-dependent effects of FF and WY on cell survival in the presence of CDDP, A549 cells were pretreated with 5-50 μM of FF, 5-50 μM of WY, or vehicle alone for 12 h, followed by exposure to 40 μM CDDP for 72 h in the presence or absence of FF or WY. Cell survival was determined using Hoechst 33342 DNA quantification assay (n=6). Data are expressed as the mean and standard error of the mean. **P<0.01 using the one-way ANOVA and Dunnett's test. (D) To study the inhibitory effect of GW on FF-induced promotion of cell survival, A549 cells were pretreated with 50 μM FF in the presence or absence of 5 μM GW for 12 h, followed by exposure to 40 μM CDDP for 72 h. Cell survival was determined by Hoechst 33342 DNA quantification assay (n=6). Data are expressed as the mean and standard error of the mean. **P<0.01 using the one-way ANOVA and Tukey-Kramer test. (E) For survival analysis of other lung cancer cells, H1299, PC3, and H441 cells were pretreated with 50 μM FF or vehicle alone for 12 h, followed by exposure to 10-80 μM of CDDP for 72 h in the presence or absence of FF. Cell survival was determined by Hoechst 33342 DNA quantification assay (n=8). *P<0.05 and **P<0.01 vs. control using the Welch t-test. FF, fenofibrate; CDDP, cisplatin; WY, WY14643; GW, GW6471.

(γH2AX) (19) (Fig. 2A and B) and phosphorylation of the p53 protein (Fig. 2C). However, the presence of FF or WY at 50 μM had no effect on the DNA damage response to CDDP. We also evaluated the expression of the Bcl-2 family proteins, which are thought to regulate apoptosis following

CDDP-induced DNA damage (20). The expression of the proapoptotic proteins Bax and Bad, as well as the antiapoptotic proteins Bcl-2 and Bcl-x, were comparable in A549 cells, regardless of exposure to CDDP and of the presence of FF and WY (Fig. 2D). These findings indicated that FF and
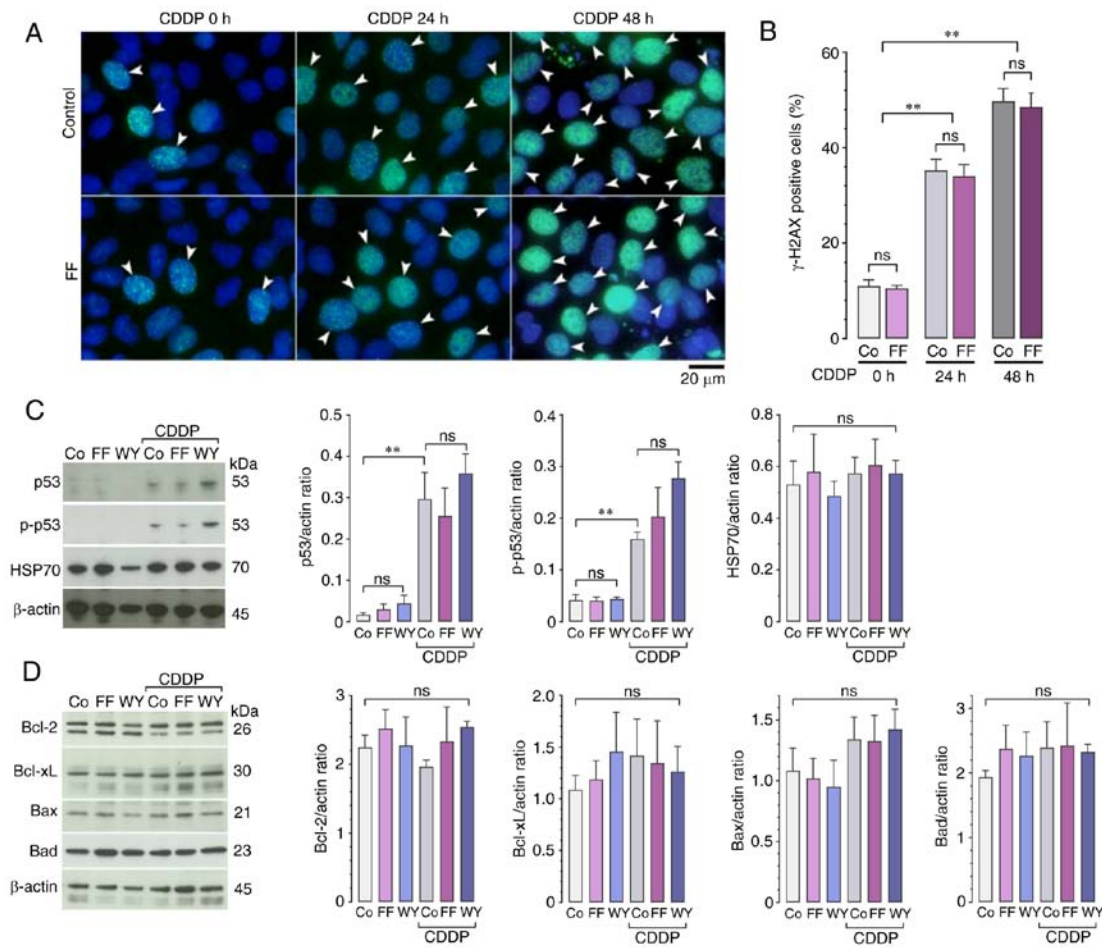
Figure 2. Effects of FF and WY on CDDP-induced DNA damage response. A549 cells were pretreated with 50 μM FF, 50 μM WY, or vehicle alone for 24 h, followed by exposure to 40 μM CDDP for 24 or 48 h (i.e., 24 h unless indicated) in the presence or absence of FF or WY. (A and B) Immunofluorescence of γH2AX expression. (A) Representative images of γH2AX expression (green); cell nuclei were counterstained with DAPI (blue); the arrowheads indicate γH2AX-positive cells. (B) The percentages of γH2AX-positive cells are shown. Data are expressed as the mean and standard error of the mean (n=4). **P<0.01 using the two-way ANOVA and Tukey-Kramer test t; ns, not significant; Co, control. (C and D) Western blot analyses for the expression of p53, p-p53, and HSP70 (C); and Bcl-2, Bcl-xL, Bax, and Bad (D) are shown. The relative protein levels were estimated using densitometry and normalized to the level of β-actin as a loading control. Data are expressed as the mean and standard error of the mean (n=4). **P<0.01 using the one-way ANOVA and Tukey-Kramer test. FF, fenofibrate; WY, WY14643; CDDP, cisplatin; γH2AX, γH2A histone family member X; DAPI, 4',6-diamidino-2-phenylindole; p-p53, phosphorylated p53; HSP70, heat shock protein 70; Bcl-2, B-cell/CLL lymphoma 2; Bcl-xL, B-cell lymphoma-extra large; Bax, Bcl-2-associated X protein; Bad, Bcl-2 antagonist of cell death.

WY did not modulate the DNA damage response elicited by CDDP. In addition, treatment of A549 cells with FF and WY had no effect on the expression of the HSP70 protein, which is thought to contribute to CDDP resistance (21), regardless of exposure to CDDP (Fig. 2C).

FF treatment reduced CDDP-induced ROS accumulation by enhancing antioxidant activity. CDDP cytotoxicity results not only from a DNA damage response but also from ROS generation (16). In this study, CDDP exposure of A549 cells increased the cellular ROS levels (Fig. 3A); this corroborated the findings of previous researches (22,23). However, the presence of FF or WY at 50 μM significantly reduced the cellular ROS levels (Fig. 3A) and promoted A549 cell survival after exposure to exogenous hydrogen peroxide (Fig. 3B). Based on these findings, we hypothesized that rather than reducing oxidant production, FF and WY enhanced the activity of antioxidants. Consistent with our expectations, FF or WY at 50 μM enhanced the protein expressions of mitochondrial

Mn SOD (SOD2), HO-1, and catalase (Fig. 4A and B), as well as the enzyme activities of SOD and catalase (Fig. 4C and D). Both FF and WY did not affect the protein expression of cytosolic Cu/Zn SOD (SOD1), which was expressed at a high level in A549 cells, regardless of exposure to FF and WY (Fig. 4A) (24). These findings indicated that FF and WY reduced cellular ROS by enhancing the antioxidant activity of A549 cells.

FF treatment enhanced the expression and activation of Nrf2 transcription factor. Next, we examined whether the enhancement of antioxidants by FF was mediated by the activation of Nrf2, which is a transcription factor that binds to the antioxidant response element (ARE) to stimulate the transcription of antioxidant genes, such as those of SOD, HO-1 and catalase (25,26). Treatment with FF or WY at 50 μM increased the transcription, translation, nuclear translocation, and sequence-specific DNA-binding activity of Nrf2 in A549 cells (Fig. 5A-D). The Nrf2 protein undergoes rapid ubiquitination
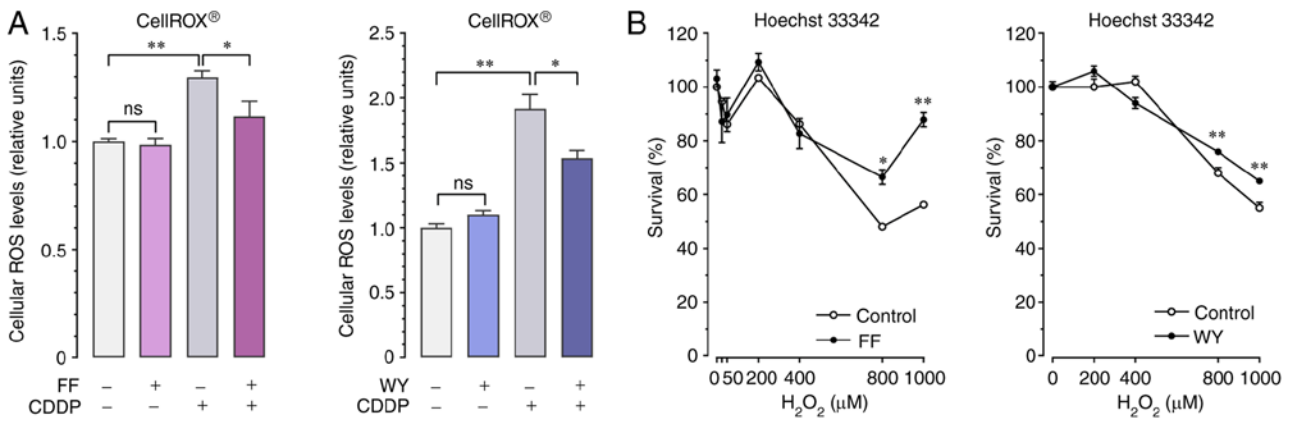
Figure 3. Effects of fenofibrate FF and WY on CDDP-induced cellular ROS accumulation and H_2O_2-induced cell death. (A) For the quantitative analysis of cellular ROS levels, A549 cells were pretreated with 50-μM FF, 50 μM WY, or vehicle alone for 12 h, followed by exposure to 40 μM CDDP for 48 h in the presence or absence of FF or WY. Cellular ROS levels were estimated using the CellROX® Green assay. Data are expressed as the mean and standard error of the mean (n=12). *P<0.05 and **P<0.01 using the one-way ANOVA and Tukey-Kramer test; ns, not significant. (B) To analyze cell survival after H_2O_2 exposure, A549 cells were pretreated with 50 μM FF, 50 μM WY, or vehicle alone for 36 h, followed by exposure to 25-1,000 μM of H_2O_2 for 48 h in the presence or absence of FF or WY. Cell survival was determined by Hoechst 33342 DNA quantification assay. Data are expressed as the mean and standard error of the mean (n=8). *P<0.05 and **P<0.01 vs. control using the Welch t-test. FF, fenofibrate; WY, WY14643; CDDP, cisplatin; ROS, reactive oxygen species.
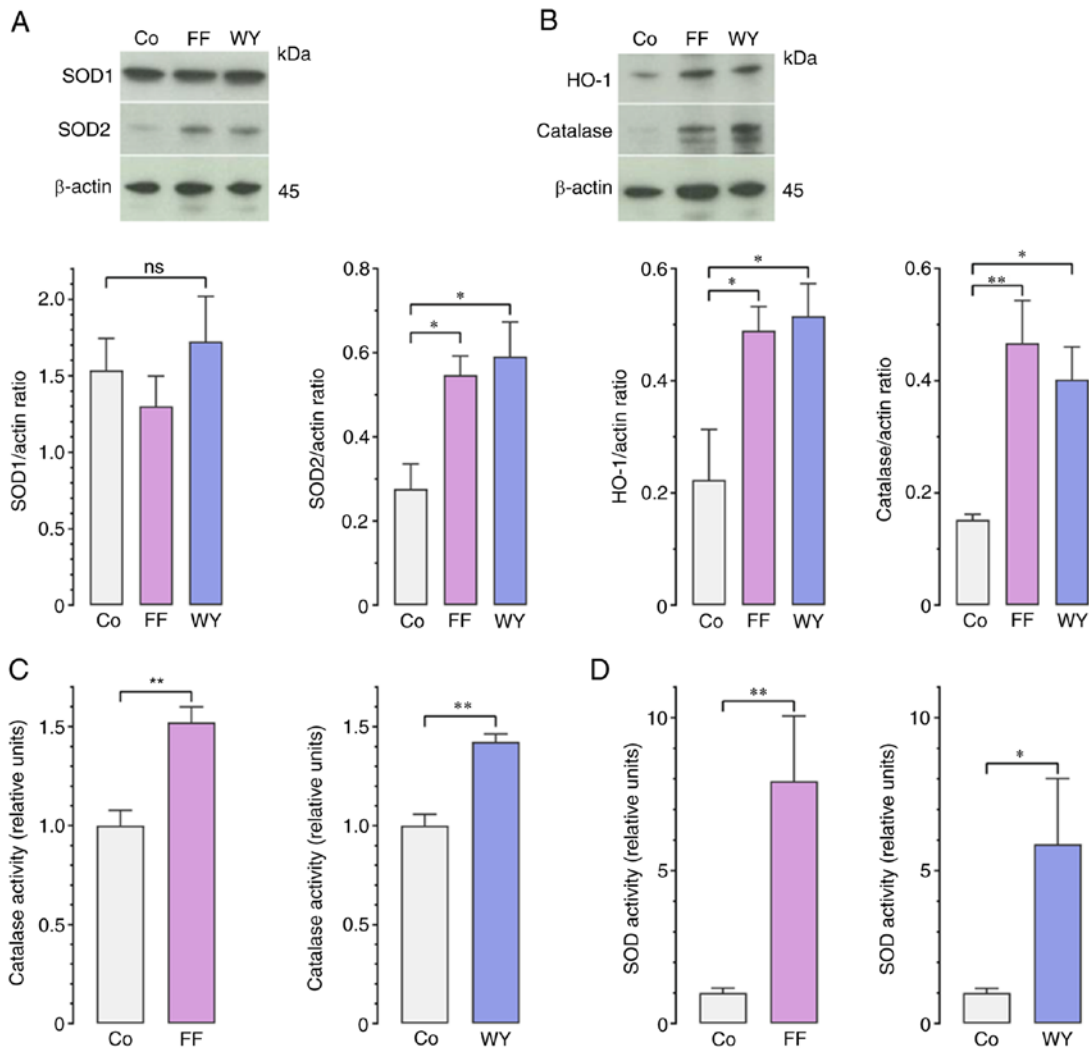

Figure 4. Effects of FF and WY on the protein expression and enzyme activity of antioxidants. A549 cells were treated with 50 μM FF, 50 μM WY, or vehicle alone for 36 h. (A) Western blot analyses for SOD 1 and SOD2 and for (B) HO-1 and catalase were done. The relative protein levels were estimated using densitometry and normalized to the protein levels of β-actin as a loading control. Data are expressed as the mean and standard error of the mean (n=4). *P<0.05 and **P<0.01 using the one-way ANOVA and Dunnett's test (n=4); ns, not significant; Co, control. (C) The enzyme activities of catalase and (D) SOD are shown. Data are expressed as the mean and standard error of the mean (n=6). *P<0.05 and **P<0.01 using the Welch t-test. FF, fenofibrate; WY, WY14643; SOD, superoxide dismutase; HO-1, heme oxygenase-1.
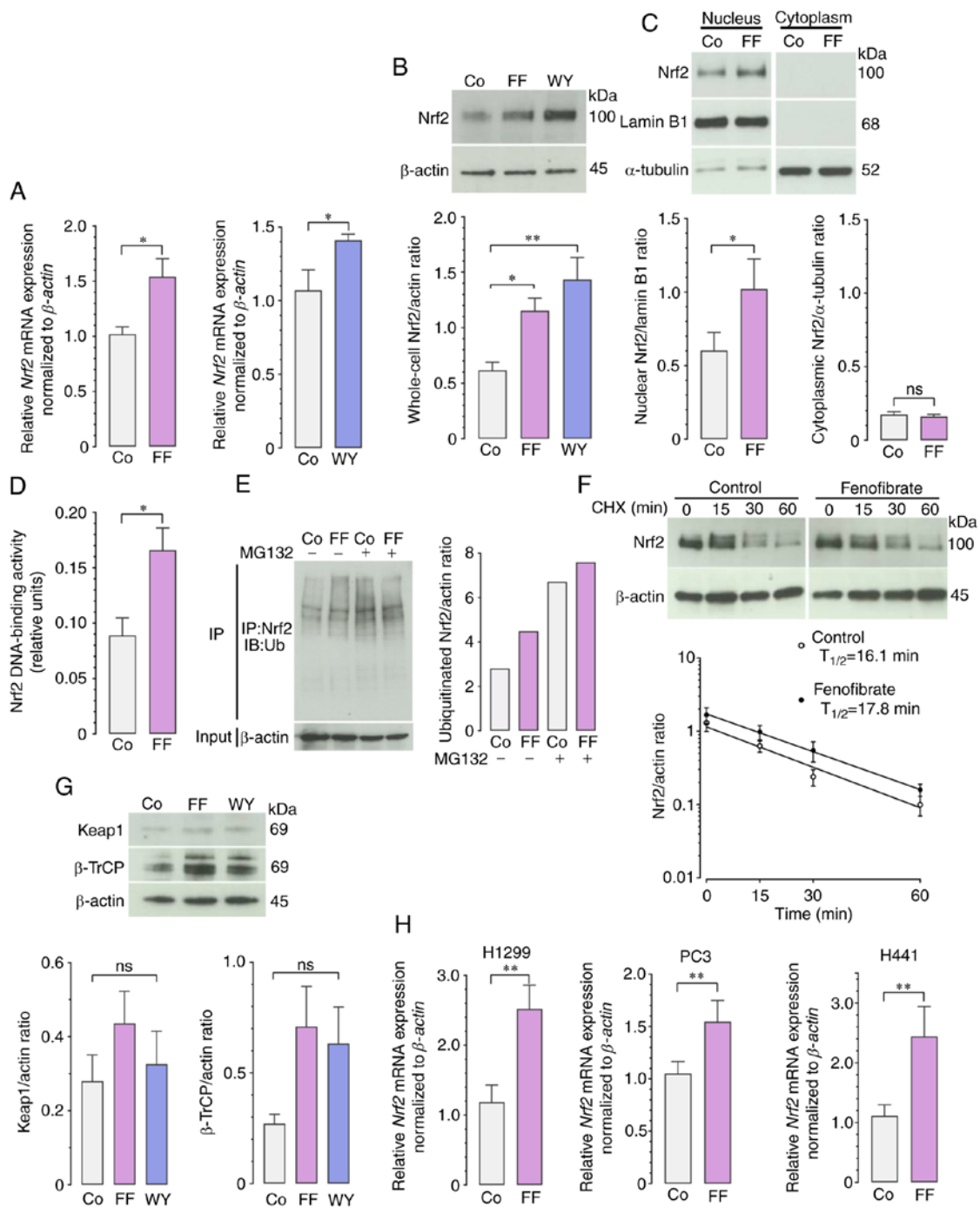
Figure 5. Effects of FF and WY on the transcription, translation, activation, and degradation of Nrf2. (A-F) A549 cells were treated with 50 μM FF, 50 μM WY, or vehicle alone for 36 h. (A) Reverse transcription-quantitative polymerase chain reaction was used to analyze *Nrf2* gene expression. The expression levels of *Nrf2* mRNA were normalized to the level of *β-actin* mRNA as a housekeeping gene. Data are expressed as the mean and standard error of the mean (n=10). *P<0.05 using the Welch t-test (n=10); Co, control. (B) Western blot analysis for whole-cell Nrf2 protein expression was done. The relative protein levels were estimated using densitometry and normalized to the level of β-actin as a loading control. Data are expressed as the mean and standard error of the mean (n=4). *P<0.05 and **P<0.01 using the one-way ANOVA and Dunnett's test. (C) Western blot analysis for nuclear and cytoplasmic Nrf2 protein was done; the relative protein levels were normalized to lamin B1 and α-tubulin, respectively. Data are expressed as the mean and standard error of the mean (n=4). *P<0.05 using the Welch t-test (n=4). (D) The sequence-specific DNA-binding activity of Nrf2 is shown. Data are expressed as the mean and standard error of the mean (n=8). *P<0.05 using the Welch t-test. (E) Ubiquitination level of Nrf2. A549 cells were treated with or without 10 μM of MG132, a protease inhibitor, 16 h before the preparation of cell lysates, which were used for the immunoprecipitation of Nrf2 using antiNrf2 antibody. The ubiquitination levels of Nrf2 were examined by immunoblotting using antiUb antibody. The levels were reduced in the absence of MG132, which was a negative control of experiments. (F) Nrf2 protein degradation was assessed by cycloheximide chase assay. A549 cells were treated with 50-μM FF for 36 h, followed by addition of 100-μg/ml cycloheximide. After 0, 15, 30, and 60 min, the cells were lysed and processed for Western blot analysis for determination of whole-cell Nrf2 protein content. The relative protein levels were estimated using densitometry, normalized to the protein levels of β-actin as a loading control, and plotted against time. Data are expressed as the standard error of the mean (n=4). (G) Western blot analysis for Keap1 and β-TrCP; the relative protein levels were normalized to the level of β-actin as loading control (n=4). (H) Reverse transcription-quantitative polymerase chain reaction was done to analyze the gene expression of *Nrf2* in H1299, PC3, and H441 cells after 12 h of treatment of with 50 μM FF. The expression levels of *Nrf2* mRNA were normalized to the level of *β-actin* mRNA as a housekeeping gene. Data are expressed as the mean and standard error of the mean (n=7-9). **P<0.01 using the Welch t-test; FF, fenofibrate; WY, WY14643; Nrf2, nuclear factor-erythroid 2-related factor 2; Ub, ubiquitinin; Keap1, Kelch-like ECH-associated protein 1; β-TrCP, β-transduction repeat containing protein; Co, control; ns, not significant.
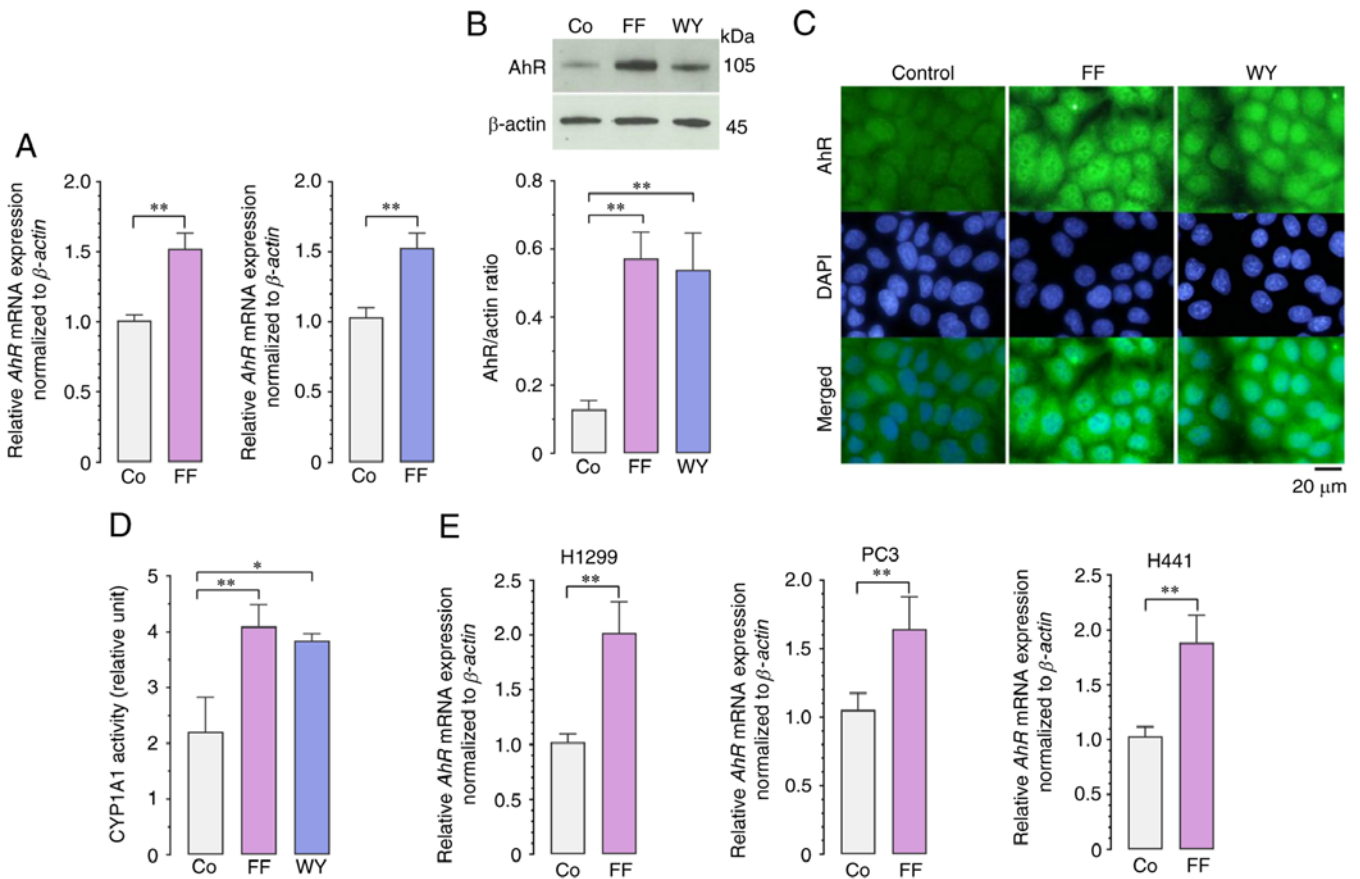
Figure 6. Effects of FF and WY on the transcription, translation, and activation of the AhR. (A-D) A549 cells were treated with 50 μM FF, 50 μM WY, or vehicle alone for 36 h. (A) Reverse transcription-quantitative polymerase chain reaction was performed to analyze *AhR* expression. The expression levels of *AhR* mRNA were normalized to the level of *β-actin* mRNA as a housekeeping gene. Data are expressed as the mean and standard error of the mean (n=10). **P<0.01 using the Welch t-test. (B) Western blot analysis for AhR protein expression was done. The relative protein levels were estimated using densitometry and normalized to the level of β-actin as a loading control. **P<0.01 using the one-way ANOVA and Dunnett's test. (C) Representative images of immunofluorescence show increased cellular expression and nuclear translocation of AhR (green) after treatment with FF or WY. Cell nuclei were counterstained with DAPI (blue). (D) Measurement of CYP1A1 activity is shown. Data are expressed as the mean and standard error of the mean (n=4). *P<0.05 and **P<0.01 using the one-way ANOVA and Dunnett's test. (E) Reverse transcription-quantitative polymerase chain reaction was performed to analyze the gene expression of *AhR* in H1299, PC3, and H441 cells after 12 h of treatment of with 50 μM FF. The expression levels of *AhR* mRNA were normalized to the level of *β-actin* mRNA as a housekeeping gene. Data are expressed as the mean and standard error of the mean (n=7-9). **P<0.01 using the Welch t-test. FF, fenofibrate; WY, WY14643; AhR, aryl hydrocarbon receptor; DAPI, 4',6-diamidino-2-phenylindole; CYP1A1, cytochrome P450 1A1; Co, control.

and proteasomal degradation upon its binding to Keap1-Cullin3 and β-TrCP-Cullin1 (27,28). Therefore, we examined whether FF affected the ubiquitination and degradation of Nrf2. Western blot analyses of Nrf2-immunoprecipitated proteins by anti-ubiquitin antibody demonstrated no significant difference in the ubiquitination level of Nrf2 in the presence and absence of FF (Fig. 5E). A cycloheximide chase assay showed similar half-lives (T$_{1/2}$) of the Nrf2 protein in the presence (17.8 min) or absence (16.1 min) of FF at 50 μM (Fig. 5F). This result indicated that FF had no effect on Nrf2 protein degradation. Furthermore, the presence of FF and WY had no effect on the protein expression of Keap1 and β-TrCP (Fig. 5G). The extremely low basal Keap1 level in A549 cells was presumably secondary to hypermethylation of the Keap1 promoter in these cells (29,30). These findings implied that treatment of A549 cells with FF enhanced the transcription, translation, and activation of Nrf2 without affecting its degradation. Consistent with those found with A549 cells, treatment with FF at 50 μM enhanced the transcription of the *Nrf2* gene in H1299, PC3, and H441 cells (Fig. 5H).

FF treatment enhanced Nrf2 expression by stimulating AhR expression. The promoter region of Nrf2 was reported to possess a xenobiotic response element (XRE) (31), which implies that the AhR can bind to the XRE after heterodimerizing with its partner AhR nuclear translocator and activate Nrf2 gene transcription (32). Furthermore, the promoter region of AhR was reported to possess PPRE (33), which implies that upon activation by FF, PPAR-α can bind to the PPRE after heterodimerizing with the retinoid X receptor and activate *AhR* gene transcription. Based on these previous researches, we examined whether the FF-induced enhancement of Nrf2 expression was secondary to a preceding enhancement of AhR expression by FF. As shown in Fig. 6A-D, treatment with FF or WY at 50 μM increased the transcription, translation, and nuclear translocation of AhR, as well as the enzyme activity of CYP1A1, which is increasingly expressed when AhR binds to the XRE (34,35). Consistent with those found with A549 cells, treatment with FF at 50 μM enhanced the transcription of the *AhR* gene in H1299, PC3, and H441 cells (Fig. 6E).
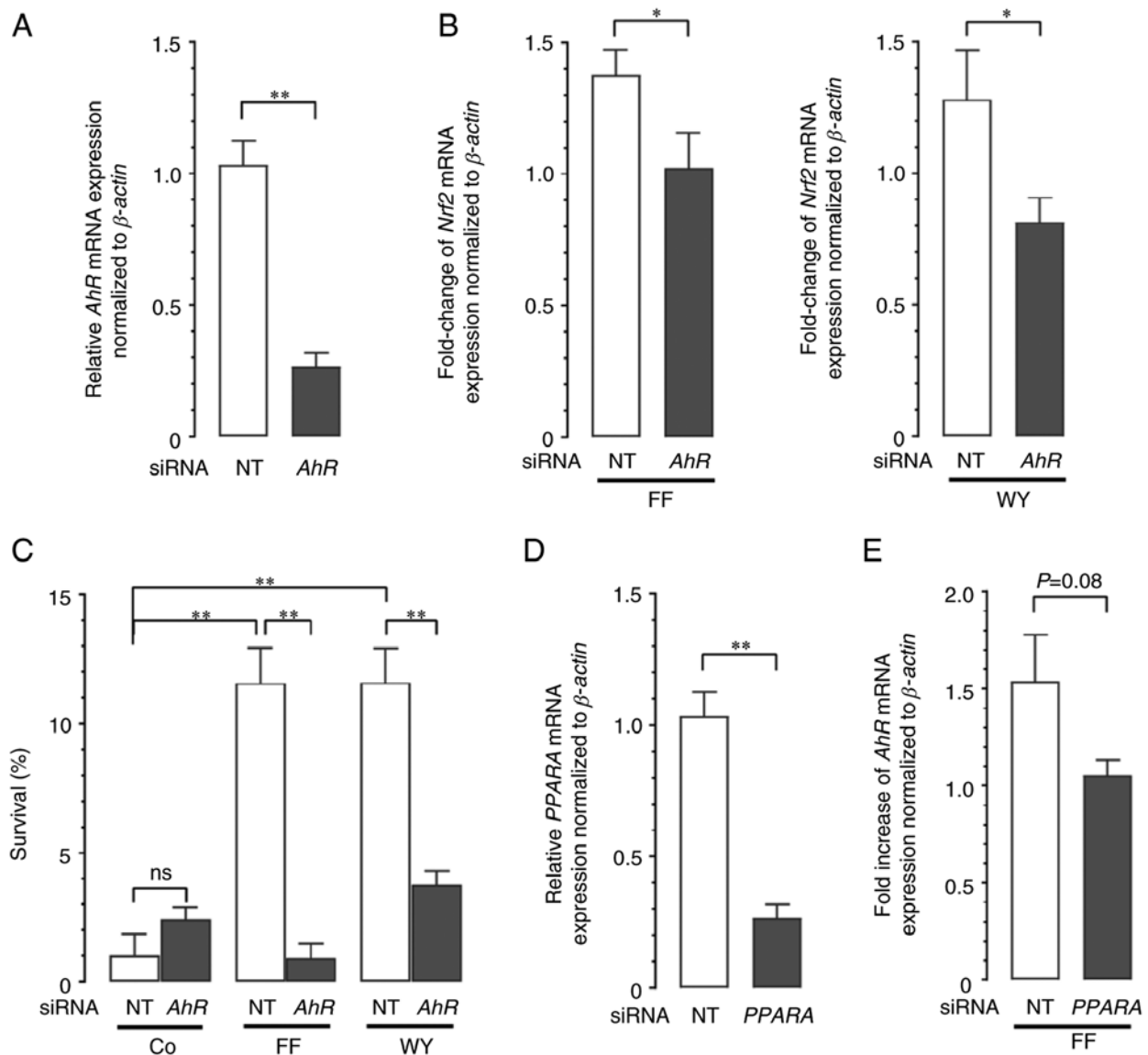
Figure 7. Effect of *AhR* gene and *PPARA* gene knockdown with siRNA. (A) Knockdown efficiency of *AhR* siRNA. A549 cells were transfected with AhR-targeting or NT siRNA. The expression levels of *AhR* mRNA at 48 h were determined by reverse transcription-quantitative polymerase chain reaction and normalized to the level of *β-actin* mRNA as a housekeeping gene. Data are expressed as the mean and standard error of the mean (n=10). **P<0.01 using the Welch t-test. (B) Effect of *AhR* gene knockdown on *Nrf2* gene expression. A549 cells were transfected with AhR-targeting or NT siRNA, followed by treatment with 50 μM FF, 50 μM WY, or vehicle alone for 36 h. The expression levels of *Nrf2* mRNA were normalized to the level of *β-actin* mRNA as a housekeeping gene. Data are expressed as the mean and standard error of the mean (n=8 for FF treatment, n=10 for WY treatment). *P<0.05 using the Welch t-test. (C) For cell survival analysis, A549 cells transfected with AhR-targeting or NT siRNA were pretreated with 50 μM FF, 50 μM WY, or vehicle alone for 12 h followed by exposure to 40 μM CDDP for 72 h in the presence or absence of FF or WY. Cell survival was determined using Hoechst 33342 DNA quantification assay. Data are expressed as the mean and standard error of the mean (n=6). **P<0.01 using the one-way ANOVA and Tukey-Kramer test. (D) Knockdown efficiency of PPARA siRNA. A549 cells were transfected with PPARA-targeting or NT siRNA. The expression levels of *PPARA* mRNA at 24 h were determined by reverse transcription-quantitative polymerase chain reaction and normalized to the level of *β-actin* mRNA as a housekeeping gene. Data are expressed as the mean and standard error of the mean (n=10). **P<0.01 using the Welch t-test. (E) Effect of *PPARA* gene knockdown on *AhR* gene expression. A549 cells were transfected with PPARA-targeting or NT siRNA, followed by treatment with 50 μM FF or vehicle alone for 12 h. The expression levels of *AhR* mRNA were normalized to the level of *β-actin* mRNA as a housekeeping gene. Data are expressed as the mean and standard error of the mean (n=8). AhR, aryl hydrocarbon receptor; PPARA, peroxisome proliferator-activated receptor-α; siRNA, small interfering RNA; NT, nontargeting; Nrf2, nuclear factor erythroid 2-related factor 2; FF, fenofibrate; WY, WY14643; CDDP, cisplatin; ns, not significant; Co, control.

Knockdown of the *AhR* gene with siRNA transfection reduced the effects of FF and WY, which would have otherwise increased Nrf2 gene transcription and promoted the survival of CDDP-exposed A549 cells (Fig. 7A-C). Accumulating evidence indicated that PPAR-α-independent mechanisms are involved in the pleiotropic effects of FF on various pathophysiological processes (36,37). However, the knockdown of the PPARA gene with siRNA transfection reduced the stimulatory effect of FF on AhR gene transcription, although the AhR gene inhibition by the PPARA siRNA transfection was not statistically significant (P=0.08) (Fig. 7D and E). These findings indicated that the PPAR-α agonists FF and WY stimulated the expression of AhR that binds to the XRE, which in turn stimulated the expression of Nrf2 that binds to ARE to activate antioxidant expression, thereby, resulting in A549 cell protection from CDDP cytotoxicity.
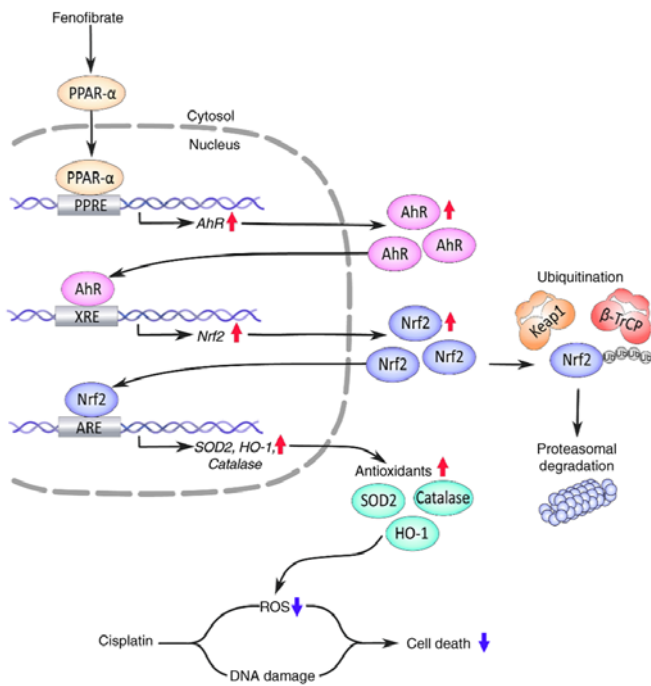
Figure 8. Graphical summary of the signaling pathway that mediates feno-fibrate (FF)-induced cytoprotection against cisplatin toxicity. ↑, increase; ↓, decrease; PPAR-α, peroxisome proliferator-activated receptor-α; PPRE, peroxisome proliferator response element; AhR, aryl hydrocarbon receptor; XRE, xenobiotic response element; Nrf2, Nuclear factor erythroid 2-related factor 2; ARE, antioxidant response element; SOD2, superoxide dismutase 2; CAT, catalase; HO-1, Heme oxygenase-1; ROS, reactive oxygen species; Keap1, Kelch-like ECH-associated protein 1; β-TrCP, β-transduction repeat containing protein; Ub, ubiquitin.

Discussion

According to previous reports, FF may have an anticancer effect (5). However, in the current study, we demonstrated that the effect of FF on lung cancer cells depended on its concentration. We discovered that FF at ≤50 μM, which is a clinically relevant blood concentration (7,18), attenuated CDDP cytotoxicity to lung cancer cells, whereas FF at ≥100 μM, albeit clinically unachievable, had an anticancer effect. The mechanism of FF attenuation of CDDP cytotoxicity involved PPAR-α-dependent AhR expression, which in turn stimulated Nrf2 expression and antioxidant production, resulting in lung cancer cell protection from CDDP-evoked oxidative damage (Fig. 8). Our findings suggested that the concomitant use of FF with CDDP may compromise the efficacy of chemotherapy.

It is understood that ROS generation contributes to CDDP cytotoxicity, whereas antioxidants generated by the Nrf2-ARE pathway cause CDDP resistance (25,38). Our findings indicate that FF attenuation of CDDP cytotoxicity was secondary to Nrf2-dependent antioxidant generation but not to the modulation of p53-dependent DNA damage response. This conclusion was supported by our observation that FF was capable of reducing CDDP cytotoxicity in p53-deficient H1299 cells and p53-proficient A549 cells.

Nrf2 activation is tightly regulated both transcriptionally and post-translationally (27,28). The posttranslational regulation of Nrf2 utilizes the Nrf2 degradation system, which is driven by E3 ubiquitin ligase complexes that involve cytosolic Keap1-Cullin3 and nuclear β-TrCP-Cullin1, which ubiquitinate and direct Nrf2 for rapid proteasomal degradation (27,28). Our findings on A549 cells showed that FF increased the Nrf2 protein by stimulating its transcription but not by affecting its degradation. These findings were contrast to those of a previous study on hepatoma cells, which showed that FF increased the Nrf2 protein post-translationally by triggering p62-dependent Keap1 degradation (39). Therefore, FF may activate Nrf2 either during transcription or after transnationally in a cell type-specific manner. In addition to Nrf2 activation, other mechanisms may underlie the FF enhancement of antioxidant activity. For example, FF may directly activate the transcription of antioxidant genes (40), because the promoter regions for the *SOD1* (41), *SOD2* (42), and *catalase* (43) genes were reported to possess the PPRE, to which PPAR-α can bind when activated by FF. In addition, FF may inhibit cellular ROS generation by interfering with the ROS-producing pathway that involves nuclear factor kappa-B and phosphoinositol 3-kinase/Akt (13,40).

Our findings indicated that FF activated the PPAR-α-PPRE-AhR-XRE-Nrf2-ARE cascade pathway to stimulate antioxidant generation. The presence of this cascade was verified by two previous gene sequence studies, which individually identified the PPAR-α-binding site PPRE in the promoter region of AhR (33) and the AhR binding site XRE in the promoter region of Nrf2 (31). Interestingly, another gene sequence study has identified the Nrf2 binding site ARE in the promoter region of AhR (44). These studies implied that the binding of AhR to XRE activates the expression of Nrf2, which binds to the ARE, thereby, allowing AhR expression in turn. This suggested the existence of a mutually synergistic interaction between Nrf2 and AhR, which may amplify the antioxidative response that is initially triggered by PPAR-α activation upon FF treatment.

In this study FF enhanced the protein expressions of mito-chondrial Mn SOD (SOD2), HO-1, and catalase. However, other antioxidants may also be involved in the FF-mediated attenuation of CDDP cytotoxicity because Nrf2 was found to stimulate the transcription of many other antioxidant genes, including SOD3, glutathione peroxidase, glutathione reductase, thioredoxin, thioredoxin reductase, and peroxiredoxin (45).

Consistent with the findings of a previous study (5), the present study found that FF had an anticancer effect. However, in our study on A549 cells, this effect required high FF concentrations of ≥100 μM, which exceed the clinically relevant blood concentrations of 50 μM (7,18). To the best of our knowledge, no previous studies administered higher doses of similar drugs in short cycles for cancer therapy; however, the present study hypothesized that higher doses of FF could be administered in short cycles with long intervals in combination with the intermittent administration of standard chemotherapeutic agents. In previous studies on different cancer cell lines, FF was found to exert an anticancer effect by inducing apoptosis, cell cycle arrest, and motility inhibition (5). Different molecular mechanisms for the anticancer effect of FF had been reported; these included the activation of AMP-activated protein kinase, fork-head box O1, and fork-head box O3A; the inhibition of Akt and extracellular-signal-regulated kinase; and the accumulation of cellular ROS (5).

Apart from the impact of FF on cancer chemotherapy, its therapeutic role as a promising antioxidant enhancer has attracted much attention (4,40). According to previous *in vitro* studies FF protected several normal cells from oxidative damage (10-13,46). Moreover, other studies using animal models of diabetic retinopathy and nephropathy, and ischemia/reperfusion-induced cardiac injury showed that FF protected these organs from damage secondary to oxidative stress in (5,47,48). However, the molecular mechanism of its antioxidative action remains unknown. The current study provided mechanistic insights into understanding the antioxidative property of FF.

In conclusion, we discovered that FF at clinically relevant concentrations attenuated CDDP cytotoxicity to lung cancer cells by enhancing the antioxidant defense system through activation of a pathway that involves the PPAR-α-PPRE-AhR-XRE-Nrf2-ARE. Although further exploration will be needed, our study suggested that in patients receiving CDDP-based chemotherapy for lung cancer, caution is required when FF is concomitantly used. Although the anticancer property of FF has recently attracted much attention, it required high FF concentrations that exceeded clinically relevant concentrations.

Availability of data and materials

The datasets used and/or analyzed during the current study are available from the corresponding author on reasonable request.

Authors' contributions

MK and KA conceived and designed the project; acquired, analyzed and interpreted the data; and wrote the original draft. SA and HN analyzed and interpreted the data. MK and KA confirm the authenticity of all the raw data. All authors read and approved the final manuscript.

Ethics approval and consent to participate

Not applicable.

Patient consent for publication

Not applicable.

Competing interest

The authors declare that they have no competing interests.

References

1. Patsouris D, Mandard S, Voshol PJ, Escher P, Tan NS, Havekes LM, Koenig W, März W, Tafuri S, Wahli W, *et al*: PPARalpha governs glycerol metabolism. J Clin Invest 114: 94-103, 2004.
2. Koltai T: Fenofibrate in cancer: Mechanisms involved in anticancer activity. F1000Res 4: 55, 2015.
3. Abdel Magid AM, Abbassi MM, Iskander EEM, Mohamady O and Farid SF: Randomized comparative efficacy and safety study of intermittent simvastatin versus fenofibrate in hemodialysis. J Comp Eff Res 6: 413-424, 2017.
4. Noonan JE, Jenkins AJ, Ma JX, Keech AC, Wang JJ and Lamoureux EL: An update on the molecular actions of fenofibrate and its clinical effects on diabetic retinopathy and other microvascular end points in patients with diabetes. Diabetes 62: 3968-3975, 2013.
5. Lian X, Wang G, Zhou H, Zheng Z, Fu Y and Cai L: Anticancer roperties of fenofibrate: A repurposing use. J Cancer 9: 1527-1537, 2018.
6. Vlase L, Popa A, Muntean D and Leucuta SE: Pharmacokinetics and comparative bioavailability of two fenofibrate capsule formulations in healthy volunteers. Arzneimittelforschung 60: 560-563, 2010.
7. Davies SP, Mycroft-West CJ, Pagani I, Hill HJ, Chen YH, Karlsson R, Bagdonaite I, Guimond SE, Stamataki Z, De Lima MA, *et al*: The hyperlipidaemic drug fenofibrate significantly reduces infection by SARS-CoV-2 in cell culture models. Front Pharmacol 12: 660490, 2021.
8. Luty M, Piwowarczyk K, Łabędź-Masłowska A, Wróbel T, Szczygieł M, Catapano J, Drabik G, Ryszawy D, Kędracka-Krok S, Madeja Z, *et al*: Fenofibrate augments the sensitivity of drug-resistant prostate cancer cells to docetaxel. Cancers (Basel) 11: 77, 2019.
9. Balakumar P, Sambathkumar R, Mahadevan N, Muhsinah AB, Alsayari A, Venkateswaramurthy N and Dhanaraj SA: Molecular targets of fenofibrate in the cardiovascular-renal axis: A unifying perspective of its pleiotropic benefits. Pharmacol Res 144: 132-141, 2019.
10. Li J, Wang P, Chen Z, Yu S and Xu H: Fenofibrate ameliorates oxidative stress-induced retinal microvascular dysfunction in diabetic rats. Curr Eye Res 43: 1395-1403, 2018.
11. Sekulic-Jablanovic M, Petkovic V, Wright MB, Kucharava K, Huerzeler N, Levano S, Brand Y, Leitmeyer K, Glutz A, Bausch A and Bodmer D: Effects of peroxisome proliferator activated receptors (PPAR)-γ and -α agonists on cochlear protection from oxidative stress. PLOS One 12: e0188596, 2017.
12. Hsu YJ, Lin CW, Cho SL, Yang WS, Yang CM and Yang CH: Protective effect of fenofibrate on oxidative stress-induced apoptosis in retinal-choroidal vascular endothelial cells: Implication for diabetic retinopathy treatment. Antioxidants (Basel) 9: 712, 2020.
13. Cortes-Lopez F, Sanchez-Mendoza A, Centurion D, Cervantes-Perez LG, Castrejon-Tellez V, Del Valle-Mondragon L, Soria-Castro E, Ramirez V, Sanchez-Lopez A, Pastelin-Hernandez G, *et al*: Fenofibrate protects cardiomyocytes from hypoxia/reperfusion- and high glucose-induced detrimental effects. PPAR Res 2021: 8895376, 2021.
14. Thongnuanjan P, Soodvilai S, Chatsudthipong V and Soodvilai S: Fenofibrate reduces cisplatin-induced apoptosis of renal proximal tubular cells via inhibition of JNK and p38 pathways. J Toxicol Sci 41: 339-349, 2016.
15. Kim SJ, Park C, Lee JN and Park R: Protective roles of fenofibrate against cisplatin-induced ototoxicity by the rescue of peroxisomal and mitochondrial dysfunction. Toxicol Appl Pharmacol 353: 43-54, 2018.
16. Dasari S and Tchounwou PB: Cisplatin in cancer therapy: Molecular mechanisms of action. Eur J Pharmacol 740: 364-378, 2014.
17. Livak KJ and Schmittgen TD: Analysis of relative gene expression data using real-time quantitative PCR and the 2(-Delta Delta C(T)) method. Methods 25: 402-408, 2001.
18. Desager JP, Horsmans Y, Vandenplas C and Harvengt C: Pharmacodynamic activity of lipoprotein lipase and hepatic lipase, and pharmacokinetic parameters measured in normolipidaemic subjects receiving ciprofibrate (100 or 200 mg/day) or micronised fenofibrate (200 mg/day) therapy for 23 days. Atherosclerosis 124 (Suppl): S65-S73, 1996.

19. Ivashkevich A, Redon CE, Nakamura AJ, Martin RF and Martin OA: Use of the γ-H2AX assay to monitor DNA damage and repair in translational cancer research. Cancer Lett 327: 123-133, 2012.

20. Yip KW and Reed JC: Bcl-2 family proteins and cancer. Oncogene 27: 6398-6406, 2008.

21. Endo H, Yano M, Okumura Y and Kido H: Ibuprofen enhances the anticancer activity of cisplatin in lung cancer cells by inhibiting the heat shock protein 70. Cell Death Dis 5: e1027, 2014.

22. Berndtsson M, Hägg M, Panaretakis T, Havelka AM, Shoshan MC and Linder S: Acute apoptosis by cisplatin requires induction of reactive oxygen species but is not associated with damage to nuclear DNA. Int J Cancer 120: 175-180, 2007.

23. Kikuchi R, Iwai Y, Tsuji T, Watanabe Y, Koyama N, Yamaguchi K, Nakamura H and Aoshiba K: Hypercapnic tumor microenvironment confers chemoresistance to lung cancer cells by reprogramming mitochondrial metabolism in vitro. Free Radic Biol Med 134: 200-214, 2019.

24. Fujii J, Homma T and Osaki T: Superoxide radicals in the execution of cell death. Antioxidants(Basel) 11: 501, 2022.

25. Shaw P and Chattopadhyay A: Nrf2-ARE signaling in cellular protection: Mechanism of action and the regulatory mechanisms. J Cell Physiol 235: 3119-3130, 2020.

26. Lee C: Collaborative power of Nrf2 and PPARγ activators against metabolic and drug-Induced oxidative injury. Oxid Med Cell Longev 2017: 1378175, 2017.

27. Kobayashi A, Kang MI, Okawa H, Ohtsuji M, Zenke Y, Chiba T, Igarashi K and Yamamoto M: Oxidative stress sensor Keap1 functions as an adaptor for Cul3-based E3 ligase to regulate proteasomal degradation of Nrf2. Mol Cell Biol 24: 7130-7139, 2004.

28. Taguchi K and Yamamoto M: The KEAP1-NRF2 system in cancer. Front Oncol 7: 85, 2017.

29. Probst BL, McCauley L, Trevino I, Wigley WC and Ferguson DA: Cancer cell growth is differentially affected by constitutive activation of NRF2 by KEAP1 deletion and pharmacological activation of NRF2 by the synthetic triterpenoid, RTA 405. PLoS One 10: e0135257, 2015.

30. Wang R, An J, Ji F, Jiao H, Sun H and Zhou D: Hypermethylation of the Keap1 gene in human lung cancer cell lines and lung cancer tissues. Biochem Biophys Res Commun 373: 151-154, 2008.

31. Miao W, Hu L, Scrivens PJ and Batist G: Transcriptional regulation of NF-E2 p45-related factor (NRF2) expression by the aryl hydrocarbon receptor-xenobiotic response element signaling pathway: Direct cross-talk between phase I and II drug-metabolizing enzymes. J Biol Chem 280: 20340-20348, 2005.

32. Larigot L, Juricek L, Dairou J and Coumoul X: AhR signaling pathways and regulatory functions. Biochim Open 7: 1-9, 2018.

33. Villard PH, Caverni S, Baanannou A, Khalil A, Martin PG, Penel C, Pineau T, Seree E and Barra Y: PPARalpha transcriptionally induces AhR expression in Caco-2, but represses AhR pro-inflammatory effects. Biochem Biophys Res Commun 364: 896-901, 2007.

34. Coelho NR, Pimpão AB, Correia MJ, Rodrigues TC, Monteiro EC, Morello J and Pereira SA: Pharmacological blockage of the AHR-CYP1A1 axis: A call for in vivo evidence. J Mol Med (Berl) 100: 215-243, 2022.

35. Terashima J, Habano W, Gamou T and Ozawa S: Induction of CYP1 family members under low-glucose conditions requires AhR expression and occurs through the nuclear translocation of AhR. Drug Metab Pharmacokinet 26: 577-583, 2011.

36. Majeed Y, Upadhyay R, Alhousseiny S, Taha T, Musthak A, Shaheen Y, Jameel M, Triggle CR and Ding H: Potent and PPARα-independent anti-proliferative action of the hypolipidemic drug fenofibrate in VEGF-dependent angiosarcomas in vitro. Sci Rep 9: 6316, 2013.

37. Kikuchi R, Maeda Y, Tsuji T, Yamaguchi K, Abe S, Nakamura H and Aoshiba K: Fenofibrate inhibits TGF-β-induced myofibroblast differentiation and activation in human lung fibroblasts in vitro. FEBS Open Bio 11: 2340-2349, 2021 (Epub ahead of print).

38. Raghunath A, Sundarraj K, Nagarajan R, Arfuso F, Bian J, Kumar AP, Sethi G and Perumal E: Antioxidant response elements: Discovery, classes, regulation and potential applications. Redox Biol 17: 297-314, 2018.

39. Park JS, Kang DH, Lee DH and Bae SH: Fenofibrate activates Nrf2 through p62-dependent Keap1 degradation. Biochem Biophys Res Commun 465: 542-547, 2015.

40. Kim T and Yang Q: Peroxisome-proliferator-activated receptors regulate redox signaling in the cardiovascular system. World J Cardiol 5: 164-174, 2013.

41. Kim YH, Yoo HY, Chang MS, Jung G and Rho HM: C/EBP alpha is a major activator for the transcription of rat Cu/Zn superoxide dismutase gene in liver cell. FEBS Lett 401: 267-270, 1997.

42. Ding G, Fu M, Qin Q, Lewis W, Kim HW, Fukai T, Bacanamwo M, Chen YE, Schneider MD, Mangelsdorf DJ, et al: Cardiac peroxisome proliferator-activated receptor gamma is essential in protecting cardiomyocytes from oxidative damage. Cardiovasc Res 76: 269-279, 2007.

43. Girnun GD, Domann FE, Moore SA and Robbins ME: Identification of a functional peroxisome proliferator-activated receptor response element in the rat catalase promoter. Mol Endocrinol 16: 2793-2801, 2002.

44. Shin S, Wakabayashi N, Misra V, Biswal S, Lee GH, Agoston ES, Yamamoto M and Kensler TW: NRF2 modulates aryl hydrocarbon receptor signaling: Influence on adipogenesis. Mol Cell Biol 27: 7188-7197, 2007.

45. Ma Q: Role of nrf2 in oxidative stress and toxicity. Annu Rev Pharmacol Toxicol 53: 401-26, 2013.

46. Sun C, Song B, Sheng W, Yu D, Yang T, Geng F, Fang K, Jiao Y, Zhang J and Zhang S: Fenofibrate attenuates radiation-induced oxidative damage to the skin through fatty acid binding protein 4 (FABP4). Front Biosci (Landmark Ed) 27: 214, 2022.

47. Kadian S, Mahadevan N and Balakumar P: Differential effects of low-dose fenofibrate treatment in diabetic rats with early onset nephropathy and established nephropathy. Eur J Pharmacol 698: 388-396, 2013.

48. Ibarra-Lara L, Sánchez-Aguilar M, Sánchez-Mendoza A, Del Valle-Mondragón L, Soria-Castro E, Carreón-Torres E, Díaz-Díaz E, Vázquez-Meza H, Guarner-Lans V and Rubio-Ruiz ME: Fenofibrate therapy restores antioxidant protection and improves myocardial insulin resistance in a rat model of metabolic syndrome and myocardial ischemia: The role of angiotensin II. Molecules 22: 31, 2016.